

Intermode coupling in a fiber loop laser at low temperatures

Eyal Buks*

Andrew and Erna Viterbi Department of Electrical Engineering, Technion, Haifa 32000, Israel

(Dated: December 12, 2023)

We experimentally study an unequally-spaced optical comb (USOC), which is generated by a unidirectional fiber loop laser operated at low temperatures. The underlying mechanism responsible for USOC formation is explored using both close and open loop measurements. The role played by dispersion is investigated using radio frequency spectrum measurements. By integrating a saturable absorber into the loop, a lasing state is revealed, in which mode locking coexists with the USOC.

Introduction - Fiber loop lasers are widely employed for a variety of applications. Commonly the loop is made of an undoped single mode fiber (SMF) section, and a doped section, which is used for optical amplification. An unequally-spaced optical comb (USOC) has been recently found in the optical spectrum of a fiber loop laser having an amplifying Erbium doped fiber (EDF), which is cooled down to cryogenic temperatures [1]. The underlying mechanism responsible for USOC formation has remained mainly unknown. Here we report on measurements, performed with both open and close loop configurations, which provide some insight into the process of USOC formation, and which allow the extraction of parameters of the fiber loop under study.

A SMF (both doped and undoped) can be characterized by a loss coefficient α , a group velocity v_g , a group velocity dispersion (GVD), and by a complex nonlinear coefficient $\gamma = \gamma' + i\gamma''$, which is proportional to the SMF third-order susceptibility [2]. The real part γ' of γ is the nonlinear dispersion coefficient [3], and the imaginary part γ'' of γ is the nonlinear absorption coefficient [4, 5]. For saturable absorption (SA) $\gamma'' < 0$, whereas $\gamma'' > 0$ for reverse saturable absorption (RSA). In a fiber loop laser, SA commonly promotes mode locking (ML) and the formation of optical pulses [6–8], whereas processes giving rise to RSA (e.g. two-photon absorption) suppress ML [9]. Changeover from SA to RSA has been observed in [10].

Fiber parameters are extracted in the current study using a variety of measurement techniques. The effect of EDF emission and absorption spectra is studied by varying the temperature and fiber loop loss. The effect of nonlinear dispersion is explored by measuring both the loop frequency as a function of optical wavelength and the lasing linewidth. Both EDF gain and nonlinear response are measured using an open loop configuration. We show that some of the experimental results can be accounted for using a simple theoretical model, which assumes that dispersion can be disregarded. However, on the other hand, this assumption is invalidated by some of our experimental results, which indicate that dispersion plays an important role.

Experimental setup - The experimental setup is described by the sketch shown in Fig. 1(a). A cryogen free cryostat is used to cool down an EDF having length denoted by l_{EDF} , absorption of 30 dB m^{-1} at 1530 nm , and mode field diameter of $6.5 \mu\text{m}$ at 1550 nm . The EDF, which is thermally coupled to a calibrated silicon diode thermometer, is pumped using a 980 nm laser diode (LD) biased with current denoted by I_D . Results are presented below for two fiber loops, one has $l_{\text{EDF}} = 10 \text{ m}$, and the other one has $l_{\text{EDF}} = 5 \text{ m}$.

The cold EDF is integrated with a room temperature fiber loop using a wavelength-division multiplexing (WDM) device. A 10:90 output coupler (OC), and two isolators [labeled by arrows in the sketch shown in Fig. 1(a)], are integrated in the fiber loop. The output port of the 10:90 OC is splitted using a 50 : 50 OC to allow probing the optical signal using both an optical spectrum analyzer (OSA) and a photodetector (PD), which is connected to either a radio frequency spectrum analyzer (RFSA), or to an oscilloscope. An optional tunable optical filter (OF) having a central wavelength denoted by λ_F , and a linewidth of $\delta_F = 1.2 \text{ nm}$ (full width at half maximum) is connected between the 50 : 50 OC and the PD.

Temperature dependency - Key properties of EDF can be controlled by varying the temperature [11–19]. EDF operating at low temperatures can be used for some applications, including multimode lasing [20, 21] and quantum information storage [22–30].

The measured optical spectrum of our device as a function of the temperature T with diode current of $I_D = 200 \text{ mA}$ is shown in Fig. 1(b). The wavelength at which lasing peaks is denoted by λ_g . The spectrum shown in Fig. 1 indicates that λ_g decreases as the temperature is lowered [31]. As is discussed below, this process is attributed to the temperature dependency of the EDF emission and absorption spectra.

Following Ref. [32], consider an infinitesimal EDF section of length dz . The signal gain along this section is expressed as $1 + \kappa dz$, where $\kappa = l_E^{-1}(1 - p_g) - l_A^{-1}p_g$, l_E^{-1} (l_A^{-1}) is the emission (absorption) inverse length (which may depend on both wavelength λ and temperature T), p_g is the ground state population fraction, and $1 - p_g$ is the excited state population fraction (note that $0 \leq p_g \leq 1$, and that due to the isotropic nature of spontaneous emission, which yields weak coupling to

*Electronic address: eyal@ee.technion.ac.il

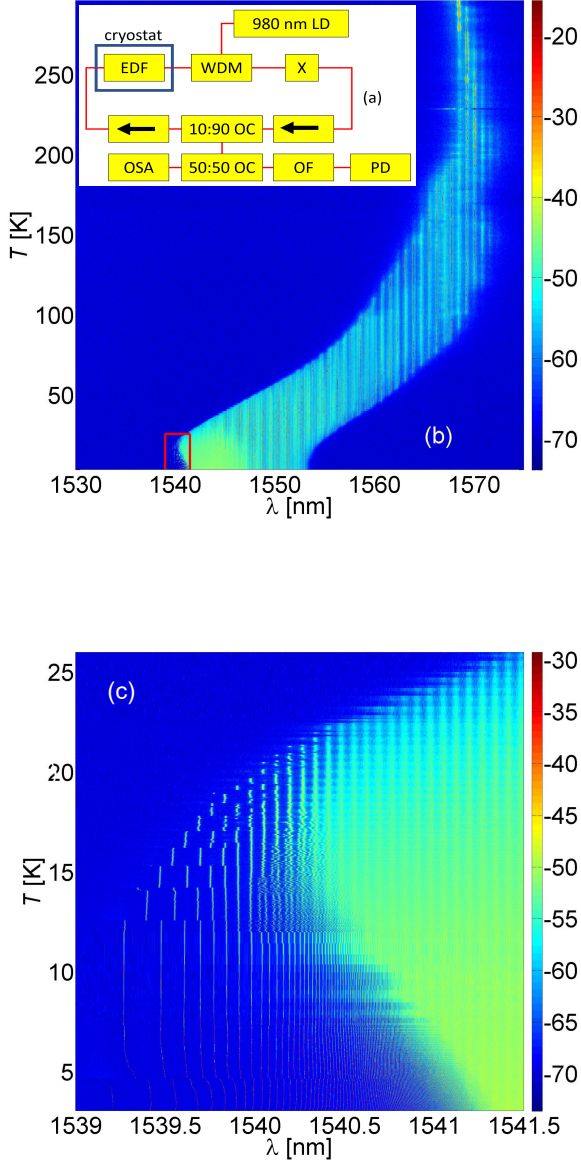


FIG. 1: Temperature dependency. (a) The experimental setup. The X box represents a tunable attenuator, which is used for the measurements presented in Fig. 2, a wavelength tunable OF, which is used for the measurements presented in Fig. 7, and a SA, which is used for the measurements presented in Fig. 8. Spectrum measurements presented in (b) and (c) are performed during cooling down. OSA data (here and in all other figures) are presented in dBm units. The EDF length is $l_{\text{EDF}} = 5$ m, and the diode current is (b) $I_{\text{D}} = 200$ mA and (c) $I_{\text{D}} = 120$ mA.

the fiber propagating mode, its contribution to the signal is disregarded). The total EDF gain g_{F} is given by $g_{\text{F}} = \exp \int_0^{l_{\text{EDF}}} \kappa dz$. The evolution of pump intensity I_{P} along the EDF is governed by $dI_{\text{P}}/dz = -l_{\text{P}}^{-1} p_{\text{g}} I_{\text{P}}$, where l_{P}^{-1} is the inverse pump decay length, thus g_{F}

can be expressed as $g_{\text{F}} = \exp(l_{\text{EDF}}/l_{\text{E}} + l_{\text{f}}^{-1} \zeta_{\text{P}})$, where $l_{\text{f}}^{-1} = l_{\text{E}}^{-1} + l_{\text{A}}^{-1}$, and where $\zeta_{\text{P}} = l_{\text{P}} \log(I_{\text{P}}(l_{\text{EDF}})/I_{\text{P}}(0))$. The total loop gain g is expressed as $g = g_{\text{F}}/\alpha_{\text{FL}}$, where $\alpha_{\text{FL}} \geq 1$ is the fiber loop loss coefficient. The lasing wavelength λ_{g} is determined from the conditions that $\log g = 0$ (i.e. $g = 1$) and $d \log g/d\lambda = 0$. By eliminating the term ζ_{P} from these two conditions one finds that $d\rho/d\lambda = 0$ at the lasing wavelength $\lambda = \lambda_{\text{g}}$, where ρ is given by

$$\rho = (\eta_{\text{EDF}} - 1) l_{\text{f}} \log \alpha_{\text{FL}}, \quad (1)$$

and where $\eta_{\text{EDF}} = l_{\text{EDF}}/(l_{\text{E}} \log \alpha_{\text{FL}})$ is the effective and normalized EDF length.

Manipulating the effective and normalized EDF length η_{EDF} by changing the loop loss coefficient α_{FL} is explored below in the next section (see Fig. 2), whereas in the current section η_{EDF} is controlled by exploiting the temperature dependence of the emission length l_{E} (see Fig. 1). As the temperature is lowered the emission length l_{E} increases, and consequently the effective and normalized EDF length η_{EDF} decreases. In the short EDF limit, for which $\eta_{\text{EDF}} \ll 1$, it is expected from the condition $d\rho/d\lambda = 0$ [see Eq. (1)] that lasing will occur in the band where emission cross section peaks near $\lambda_{\text{g}} \simeq 1540$ nm [33–36]. This behavior is demonstrated by the plot shown in Fig. 1(b) for temperatures below 10 K. The overlaid red rectangle in Fig. 1(b) indicates the region shown in Fig. 1(c) with higher resolution, inside which USOC occurs.

Attenuator - To explore the dependency on the loop loss α_{FL} coefficient, a tunable attenuator is integrated into the loop [in the location of the X-box shown in Fig. 1(a)]. The plot in Fig 2, which displays the measured optical spectrum as a function of attenuation, demonstrates the strong USOC dependence on loop loss α_{FL} . This dependency diminishes as the wavelength increases.

The condition $d\rho/d\lambda = 0$ implies in the short EDF limit that $(d\lambda_{\text{g}}/d\alpha_{\text{FL}})^{-1} = -\alpha_{\text{FL}} \log \alpha_{\text{FL}} (\log l_{\text{f}})'$, where prime denotes a derivative with respect to wavelength λ [see Eq. (1)]. This relation together with the experimental results shown in Fig. 2 yield the value of $1/(\log l_{\text{f}})' = 0.3$ nm. Note that this value is about 10 times smaller than the value of $1/(\log l_{\text{f}})'$ that is extracted from room temperature absorption and emission measurements that are reported in Ref. [32] for a similar EDF.

USOC - The USOC n 'th peak wavelength is denoted by λ_n , where $n = 0, 1, 2, \dots$ [see Fig. 1(c) and Fig. 3(a)]. The frequency f_n associated with the n 'th peak is given by $f_n = c/\lambda_n$, where c is the speed of light in vacuum, and the corresponding normalized frequency detuning i_n is defined by $i_n \equiv (f_0 - f_n)/f_{\text{L}}$, where $f_{\text{L}} = c/(n_{\text{F}} l_{\text{L}})$ is the loop frequency, $n_{\text{F}} = 1.45$ is the fiber refractive index, and l_{L} is the fiber loop total length.

The detuning sequence $\{i_n\}$ is found to be well describe by the following empirical law [1]

$$i_n = \nu \log p_n, \quad (2)$$

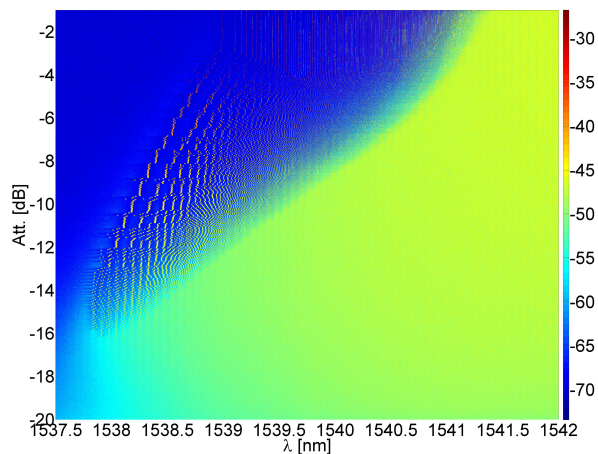


FIG. 2: In loop attenuator. The EDF length is $l_{\text{EDF}} = 5$ m, the temperature is $T = 2.8$ T, and diode current is $I_D = 150$ mA. Attenuation is changed from high (-20 dB) to low (-1 dB).

where ν is a positive constant, and p_n is the n 'th prime number. The comparison between the measured values of i_n and the calculated values of $\nu \log p_n$ [see Eq. (2)] yields a good agreement [see Fig. 3 (b)]. The level of disagreement is quantified by the parameter $\varepsilon = n_m^{-1} \sum_{n=1}^{n_m} |(i_n - \nu \log p_n) / i_n|$, where n_m is the number of peaks that can be reliably resolved. The level of disagreement ε is shown in Fig. 3 (c) as a function of the elapsed time t after switching on the diode current. The plot reveals that during the first 10 minutes after switching on the disagreement parameter ε rapidly drops down towards a value of about 0.005.

As can be seen from the empirical law given by Eq. (2), all frequency spacings $f_{n'} - f_{n''}$ between pairs of USOC peaks are unique [recall the fundamental theorem of arithmetic, and that $\log x + \log y = \log(xy)$]. As is discussed below, this observation suggests a connection between USOC formation and intermode coupling. The loop optical complex amplitude at time t is expressed as $g(f_L t)$, where the function $g(x)$ is Fourier expanded as $g(x) = \sum_{n=-\infty}^{\infty} c_n e^{2\pi i n x}$, where c_n is the complex amplitude of the n 'th loop mode. When dispersion can be disregarded, the time evolution of the (assumed slowly varying) amplitude c_n is governed by $\dot{c}_n = -\partial_n^* \mathcal{H} + \xi_n$, where ∂_n denotes the Wirtinger derivative for the n 'th mode, and where the terms ξ_n represent noise [37]. The contribution of intermode coupling to the total Hamiltonian function \mathcal{H} is given by $\mathcal{H}_c = (\gamma'' v_g / 2) \|g\|_4^4$, where $\|g\|_p$ denotes the L_p norm of g . Note that $\|g\|_2^2$ is the total optical intensity, and that $\|g\|_4^4 = \sum_{n'-n''+n'''-n''''=0} c_{n'} c_{n''}^* c_{n'''} c_{n''''}^*$. It was shown in Ref. [1] that for a fixed $\|g\|_2^2$ (total optical intensity), $\|g\|_4^4$ is nearly minimized when USOC is formed, provided that $\gamma'' > 0$ (i.e. RSA occurs in the USOC band). This observation suggests a connection between USOC forma-

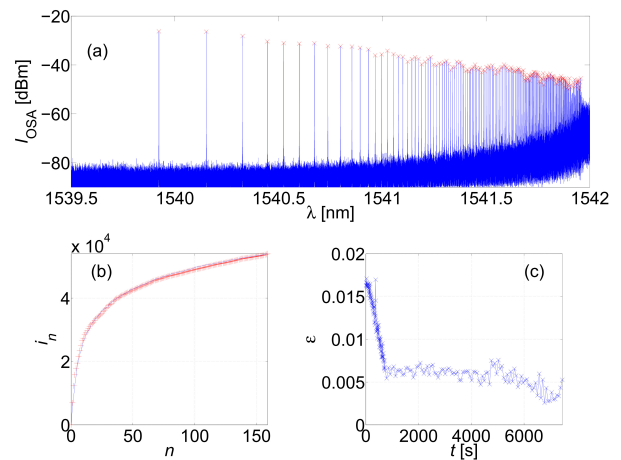


FIG. 3: USOC. (a) OSA signal I_{OSA} as a function of wavelength λ . EDF length is $l_{\text{EDF}} = 10$ m, diode current is $I_D = 200$ mA, and temperature is $T = 3.2$ K. (b) The measured values of normalized frequency detuning $i_n = (f_0 - f_n) / f_L$ (red cross symbols), and the calculated values of $\nu \log p_n$ with $\nu = 7888$ (blue solid line) [see Eq. (2)]. (c) The level of disagreement ε [of fitting using Eq. (2)] as a function of the elapsed time t after switching on the diode current.

tion and RSA, however, it has remained unclear how the assumption that dispersion can be disregarded can be justified.

Typically, USOC is highly stable and nearly temperature independent below about 5 K [see Fig. 1(b)]. In contrast, strong temperature dependency and significant drift in time of USOC peaks are observed at higher temperatures.

Further insight can be gained from the degree of polarization (DOP) of light emitted from the output port. DOP is measured by integrating a rotating quarter wave plate with the coherent optical spectrum analyzer. Using this method we find a DOP value of about 0.1 in both USOC and in the continuous (above 1542 nm) lasing bands. Note that commonly DOP is below about 0.15 in fiber lasers, unless a polarization-maintaining fiber is used [38].

RF spectrum - Further insight can be gained from probing the PD signal using a RFSA [see Fig. 1(a)]. The RF spectrum shown in Fig. 4(a) and (b), which is taken *without* the tunable OF [see Fig. 1(a)], contains an equally spaced comb of peaks centered at frequencies $n_L f_L$, where $f_L = 4.705$ MHz is the loop frequency, and where n_L is a positive integer (peaks with $n_L \lesssim 2500$ can be resolved). The measured first harmonic peak (i.e. $n_L = 1$) is shown in Fig. 4(c) as a function of the tunable OF wavelength λ_F . This plot reveals that the measured value of the loop frequency f_L inside the USOC band ($\lambda_F \lesssim 1542$ nm) drops well below its measured value in the continuous band ($\lambda_F \gtrsim 1542$ nm).

The observed drop of f_L in the USOC band can be generally attributed to both chromatic and nonlinear dis-

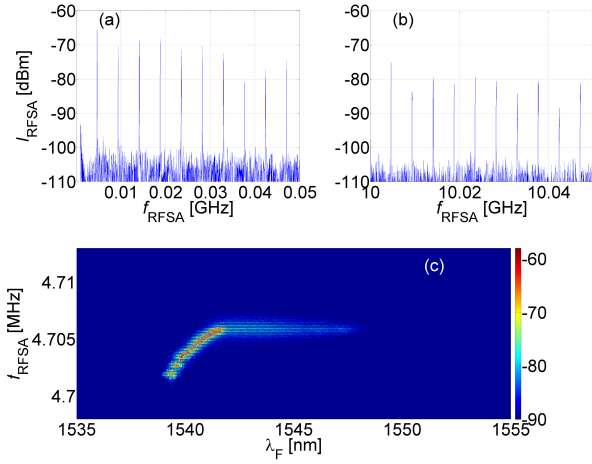


FIG. 4: RFSAs. The measurements presented in (a) and (b) are performed without the tunable OF. EDF length is $l_{\text{EDF}} = 10$ m, diode current is $I_D = 200$ mA, and temperature is $T = 4.1$ K. (c) The measured first harmonic peak (in dBm units) as a function of the tunable OF wavelength λ_F .

persion. The contribution of chromatic dispersion can be estimated from the wavelength dependency of the EDF absorption coefficient α_{EDF} [12]. The Kramers-Krönig formula, which relates α_{EDF} and the EDF refractive index n_{EDF} through a Hilbert transform [3, 36, 39–41], can be used to calculate n_{EDF} , which, in turn, yields the corresponding group index [42]. Comparing the calculated group index to the data shown in Fig. 4(c) indicates that the observed drop in f_L is far larger and far sharper compared to what is theoretically expected (when only chromatic dispersion is taken into account). This observation leads to the conclusion that the contribution of chromatic dispersion to the observed drop is relatively small. In other words, the dominant underlying mechanism responsible for the observed drop in f_L inside the USOC band is nonlinear dispersion, which is characterized by the real part γ' of the nonlinear coefficient γ .

EDF gain - Open loop measurements are performed in order to characterize the EDF gain g_{EDF} , and intermodulation response (see next section). In these measurements the loop is opened in the location of the X-box shown in Fig. 1(a).

To measure the EDF gain, a narrow band laser having a tunable wavelength λ_L is employed. Open loop EDF gain g_{EDF} is plotted in Fig. 5 as a function of wavelength λ for different values of the laser input power P_{in} . For the band $\lambda \gtrsim 1535$ nm, the measured EDF gain g_{EDF} decreases as the optical input power P_{in} is increased (see Fig. 5). This observation suggests that RSA and gain saturation occur in this wavelength band (inside which USOC is observed when the loop is closed).

Intermodulation - The technique of intermodulation is employed to characterize intermode coupling. In this technique two (phase locked) monochromatic tones are

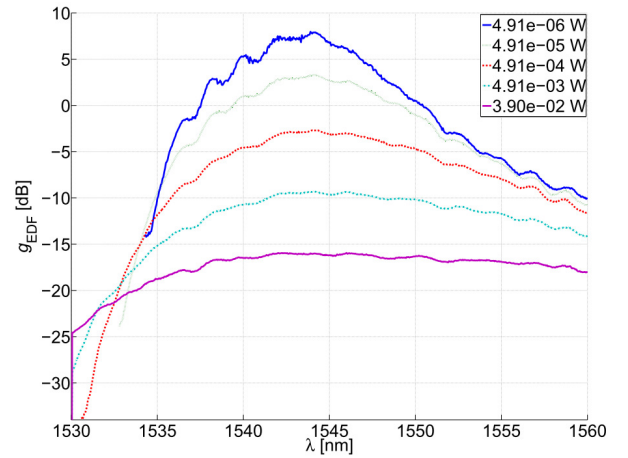


FIG. 5: EDF gain. EDF length is $l_{\text{EDF}} = 10$ m, diode current is $I_D = 150$ mA, and temperature is $T = 2.9$ K. Open loop EDF gain g_{EDF} as a function of wavelength λ for different values of the laser input power P_{in} (values of P_{in} are indicated by the figure legend).

injected into the system under study (i.e. the EDF). The first one, which has a relatively large amplitude, and a wavelength denoted by λ_p , is commonly referred to as the *pump*. The second one is a relatively low-amplitude *signal* tone having wavelength $\lambda_s = \lambda_p - \lambda_d$, where λ_d is the detuning wavelength, which is assumed to be small $|\lambda_d| \ll \lambda_p$. A driven ferrimagnetic sphere resonator is employed for the generation of this two-tone input signal [43] [see Fig. 6(a)].

Frequency mixing between the pump and signal input tones occurring in the EDF gives rise to an *idler* tone at the output [see Fig. 6(b)]. The intensity of the idler peak at wavelength $\lambda_i = \lambda_p + \lambda_d$ is shown in Fig. 6(c) as a function of pump wavelength λ_p and diode current I_D . The results presented in Fig. 6(c) suggest that intermode coupling is relatively strong in the region where USOC occurs.

The intermodulation gain $g_I \equiv P_i/P_s$, is the ratio between the generated idler power P_i and the input signal power P_s [44]. The intermodulation gain g_I is expected to depend on the nonlinear dispersion coefficient γ' . Measurements of EDFs similar to the ones used in the current study yield values for γ' in the range of $2 - 30 \text{ W}^{-1} \text{ km}^{-1}$ (at room temperature, and in the telecom band) [2, 45, 46]. On the other hand, when nonlinear absorption γ'' is disregarded, the extraction of γ' from the measured intermodulation gain g_I [see Fig. 6(c)] and the EDF gain g_{EDF} (see Fig. 5) yields values for γ' at least one order of magnitude larger (in the band where USOC occurs). This observation suggests that other nonlinear processes (e.g. nonlinear absorption) play an important role in the optical band where USOC is formed (when the loop is closed).

In loop OF - Nonlinear dispersion tends to broaden

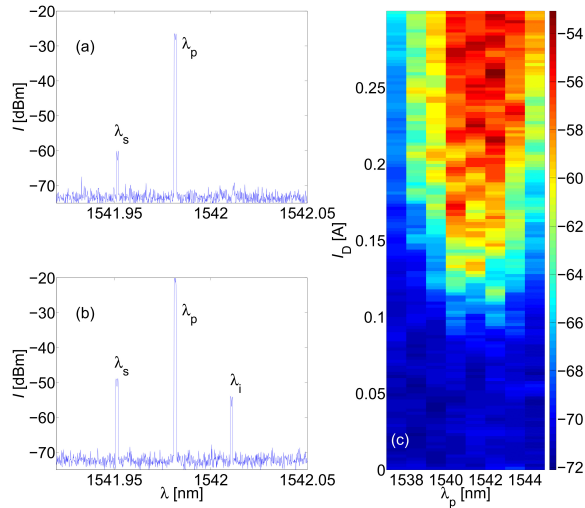


FIG. 6: Intermodulation gain - EDF length is $l_{\text{EDF}} = 10$ m, and temperature is $T = 2.9$ K. (a) The two-tone input spectrum generated using a driven ferrimagnetic sphere resonator [43]. (b) The output spectrum. (c) The idler (wavelength λ_i) peak intensity (in dBm units) as a function of pump wavelength λ_p and diode current I_D .

lasing linewidth [46–49]. To explore this, an OF having a tunable wavelength λ_F , and linewidth of $\delta_F = 1.2$ nm, is integrated into the fiber loop [in the location of the X-box shown in Fig. 1(a)].

The lasing linewidth δ_L is related to the nonlinear dispersion coefficient γ' by

$$\delta_L = \sqrt{\gamma' l_L P_C} \delta_F, \quad (3)$$

where P_C is the intra-cavity optical power [47]. This relation allows the extraction of γ' from the measured lasing linewidth δ_L . The measured optical spectrum is shown in Fig. 7 as a function of λ_F . The region where λ_F is tuned to the band where USOC is formed (in the absence of the OF) is shown in higher resolution in the inset of Fig. 7. The measured lasing linewidth δ_L is about 2 pm in the range $\lambda_F \in [1548 \text{ nm}, 1565 \text{ nm}]$, whereas $\delta_L \simeq 200 - 500$ pm for λ_F in the band where USOC occurs (in the absence of the OF) [see Fig. 1(b)]. The relation (3) yields the value of $\gamma' = 1.4 \text{ W}^{-1} \text{ km}^{-1}$ for the range $\lambda_F > 1548$ nm, whereas significantly larger values for γ' are obtained for the band where USOC occurs. This observation further supports the hypothesis that other nonlinear processes play an important role in the band where USOC is formed [note that nonlinear absorption is disregarded in the derivation of Eq. (3)].

SA - To further explore the role played by nonlinear absorption (characterized by the imaginary part γ'' of the nonlinear coefficient γ), a SA made of graphite [50, 51] is integrated into the fiber loop [in the location of the X-box shown in Fig. 1(a)]. The measured optical spectrum is shown as a function of diode current I_D in Fig 8(a).

The USOC region is shown in higher resolution in Fig 8(b).

The effect of the integrated SA is explored by measuring PD time traces for different values of the OF wavelength λ_F [see Fig. 8(c)]. Note that the OF is installed outside the loop [see Fig. 1(a)]. The periodic short pulses that are shown in Fig. 8(c3) and (c4) indicate that ML occurs in the continuous band ($\lambda_F \gtrsim 1542$ nm). On the other hand, inside the USOC band ($\lambda_F \lesssim 1542$ nm) no pulses are observed [see Fig. 8(c1) and (c2)], thus the USOC band does not participate in the ML. The observed coexistence of USOC and ML suggests that the coupling between the USOC and continuous bands is relatively weak. This weakness is partially attributed to the above-discussed drop in the loop frequency f_L that is observed in the USOC band [see Fig. 4(c)], which, in turn, gives rise to phase mismatch [52, 53], and suppression of coherent coupling between the USOC and continuous bands [54–56].

Discussion - Further study is needed to reveal the underlying mechanisms responsible for USOC formation. On the one hand, a simple theoretical model that disregards dispersion, suggests a connection between USOC formation and RSA. On the other hand, our experimental findings invalidate the assumption that dispersion can be disregarded. Theoretical modeling of the system under study is highly challenging in the presence of dispersion, because explicit time dependency cannot be eliminated by a transformation into a rotating frame. Future work will be devoted for the development of a theory capable of quantitatively reproducing the highly rich and convoluted behaviors that are experimentally observed.

Acknowledgments - Useful discussions with Luca Leuzzi, Vassilios Kovanis and Kerry Vahala are acknowledged. We thank Michael Shlafman for his help in graphite preparation.

Disclosures - The authors declare no conflicts of in-

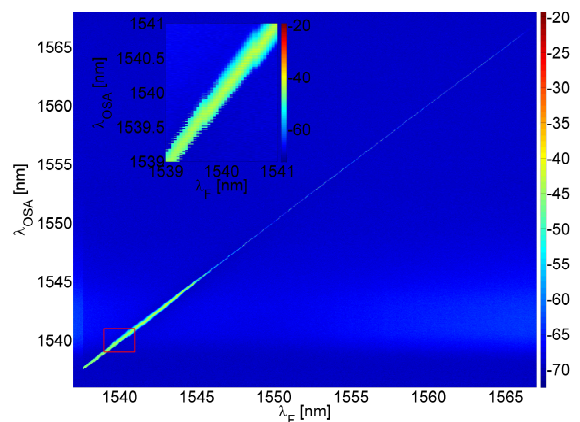


FIG. 7: In loop OF. EDF length is $l_{\text{EDF}} = 10$ m, diode current is $I_D = 120$ mA, and temperature is $T = 2.9$ K.

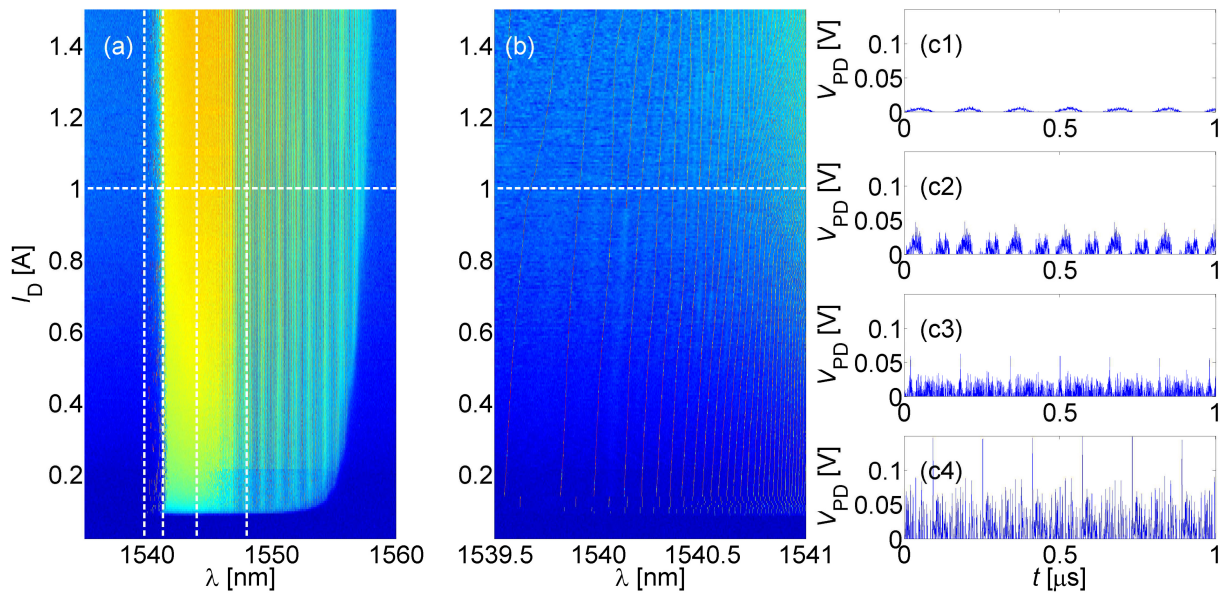


FIG. 8: Graphite SA. EDF length is $l_{\text{EDF}} = 5$ m, and temperature is $T = 3.2$ T. OF wavelength [labeled by vertical dotted lines in (a)] is (c1) $\lambda_F = 1539.8$ nm, (c2) $\lambda_F = 1541.3$ nm, (c3) $\lambda_F = 1544$ nm and (c4) $\lambda_F = 1548$ nm, and diode current [labeled by horizontal dotted lines in (a) and (b)] for the time traces shown in (c1), (c2), (c3) and (c4) is $I_D = 1000$ mA.

terest.

-
- [1] Eyal Buks, “Low temperature spectrum of a fiber loop laser”, *Physics Letters A*, vol. 458, pp. 128591, 2023.
- [2] Govind P Agrawal, “Nonlinear fiber optics”, in *Nonlinear Science at the Dawn of the 21st Century*, pp. 195–211. Springer, 2000.
- [3] M Montagna, S Selleri, and M Zoboli, “Nonlinear refractive index in erbium-doped optical amplifiers”, *Optical and quantum electronics*, vol. 27, pp. 871–880, 1995.
- [4] Deeksha Jachpure and R Vijaya, “Saturable absorption and its consequent effects in bistable erbium-doped fiber ring laser”, *Journal of Optics*, vol. 24, no. 2, pp. 024007, 2022.
- [5] Yoshinobu Maeda, “Mechanism of the negative nonlinear absorption effect in a five-level system of the Er^{3+} ion”, *Journal of applied physics*, vol. 83, no. 3, pp. 1187–1194, 1998.
- [6] Todd Kapitula, J Nathan Kutz, and Björn Sandstede, “Stability of pulses in the master mode-locking equation”, *JOSA B*, vol. 19, no. 4, pp. 740–746, 2002.
- [7] Michael L Dennis and Irl N Duling, “Experimental study of sideband generation in femtosecond fiber lasers”, *IEEE Journal of Quantum electronics*, vol. 30, no. 6, pp. 1469–1477, 1994.
- [8] Shen Huang, Guodong Shao, Yufeng Song, Luming Zhao, Deyuan Shen, and Dingyuan Tang, “Dark solitons embedded in a stable periodic pulse train emitted by a fiber ring laser”, *Journal of Physics: Photonics*, vol. 2, no. 3, pp. 034009, 2020.
- [9] Gang Wang, Yuxuan Ma, Ce Shang, Haojing Huang, Zherui Lu, Shuaixin Wang, Jingxuan Sun, Chenghong Zhang, and Bo Fu, “Influence of reverse saturable absorption effect on conventional and dissipative solitons fiber lasers”, *Optics & Laser Technology*, vol. 137, pp. 106805, 2021.
- [10] Rongfei Wei, Hang Zhang, Xiangling Tian, Tian Qiao, Zhongliang Hu, Zhi Chen, Xin He, Yongze Yu, and Jianrong Qiu, “Mos 2 nanoflowers as high performance saturable absorbers for an all-fiber passively q-switched erbium-doped fiber laser”, *Nanoscale*, vol. 8, no. 14, pp. 7704–7710, 2016.
- [11] Andrey Kobayakov, Michael Sauer, and Dipak Chowdhury, “Stimulated brillouin scattering in optical fibers”, *Advances in optics and photonics*, vol. 2, no. 1, pp. 1–59, 2010.
- [12] Julien Le Gouët, Jérémy Oudin, Philippe Perrault, Alaeddine Abbes, Alice Odier, and Alizée Dubois, “On the effect of low temperatures on the maximum output power of a coherent erbium-doped fiber amplifier”, *Journal of Lightwave Technology*, vol. 37, no. 14, pp. 3611–3619, 2019.
- [13] Luc Thevenaz, Alexandre Fellay, Massimo Facchini, Walter Scandale, Marc Nikles, and Philippe A Robert, “Brillouin optical fiber sensor for cryogenic thermometry”, in *Smart Structures and Materials 2002: Smart Sensor Technology and Measurement Systems*. International Society for Optics and Photonics, 2002, vol. 4694, pp. 22–27.
- [14] Marine Aubry, Luciano Mescia, Adriana Morana,

- Thierry Robin, Arnaud Laurent, Julien Mekki, Emmanuel Marin, Youcef Ouerdane, Sylvain Girard, and Aziz Boukenter, “Temperature influence on the radiation responses of erbium-doped fiber amplifiers”, *physica status solidi (a)*, vol. 218, no. 15, pp. 2100002, 2021.
- [15] João Paulo Lebarck Pizzaia, Rodolpho Ladislau Silva, Arnaldo Gomes Leal-Junior, and Carlos Eduardo Schmidt Castellani, “Temperature sensor based on an erbium-doped fiber sagnac interferometer”, *Applied Optics*, vol. 61, no. 9, pp. 2352–2356, 2022.
- [16] Haochong Liu, Wei He, Yantao Liu, Yunhui Dong, and Lianqing Zhu, “Erbium-doped fiber laser based on femtosecond laser inscribed fbg through fiber coating for strain sensing in liquid nitrogen environment”, *Optical Fiber Technology*, vol. 72, pp. 102988, 2022.
- [17] J Lopez, H Kerbertt, M Plata, E Hernandez, and S Stepanov, “Two-wave mixing in erbium-doped-fibers with spectral-hole burning at 77k”, *Journal of Optics*, vol. 22, no. 8, pp. 085401, 2020.
- [18] Andris Antuzevics, “Epr characterization of erbium in glasses and glass ceramics”, *Low Temperature Physics*, vol. 46, no. 12, pp. 1149–1153, 2020.
- [19] Tongwei Chu, Pengpeng Wang, and Cunguang Zhu, “Modeling of active fiber loop ring-down spectroscopy considering gain saturation behavior of edfa”, *Journal of Lightwave Technology*, vol. 38, no. 4, pp. 966–973, 2020.
- [20] Rosa Ana Perez-Herrera, Manuel Lopez-Amo, SW Harun, and H Arof, “Multi-wavelength fiber lasers”, in *Current Developments in Optical Fiber Technology*. In-Tech, 2013.
- [21] Hermann Haken, *Laser light dynamics*, vol. 2, North-Holland Amsterdam, 1985.
- [22] Erhan Saglamyurek, Jeongwan Jin, Varun B Verma, Matthew D Shaw, Francesco Marsili, Sae Woo Nam, Daniel Oblak, and Wolfgang Tittel, “Quantum storage of entangled telecom-wavelength photons in an erbium-doped optical fibre”, *Nature Photonics*, vol. 9, no. 2, pp. 83–87, 2015.
- [23] Matthias U Staudt, Sara R Hastings-Simon, Mikael Afzelius, Didier Jaccard, Wolfgang Tittel, and Nicolas Gisin, “Investigations of optical coherence properties in an erbium-doped silicate fiber for quantum state storage”, *Optics Communications*, vol. 266, no. 2, pp. 720–726, 2006.
- [24] Shi-Hai Wei, Bo Jing, Xue-Ying Zhang, Jin-Yu Liao, Hao Li, Li-Xing You, Zhen Wang, You Wang, Guang-Wei Deng, Hai-Zhi Song, et al., “Storage of 1650 modes of single photons at telecom wavelength”, *arXiv:2209.00802*, 2022.
- [25] Antonio Ortu, Jelena V Rakonjac, Adrian Holzäpfel, Alessandro Seri, Samuele Grandi, Margherita Mazzera, Hugues de Riedmatten, and Mikael Afzelius, “Multi-mode capacity of atomic-frequency comb quantum memories”, *Quantum Science and Technology*, vol. 7, no. 3, pp. 035024, 2022.
- [26] Duan-Cheng Liu, Pei-Yun Li, Tian-Xiang Zhu, Liang Zheng, Jian-Yin Huang, Zong-Quan Zhou, Chuan-Feng Li, and Guang-Can Guo, “On-demand storage of photonic qubits at telecom wavelengths”, *arXiv:2201.03692*, 2022.
- [27] Lucile Veissier, Mohsen Falamarzi, Thomas Lutz, Erhan Saglamyurek, Charles W Thiel, Rufus L Cone, and Wolfgang Tittel, “Optical decoherence and spectral diffusion in an erbium-doped silica glass fiber featuring long-lived spin sublevels”, *Physical Review B*, vol. 94, no. 19, pp. 195138, 2016.
- [28] Erhan Saglamyurek, Thomas Lutz, Lucile Veissier, Morgan P Hedges, Charles W Thiel, Rufus L Cone, and Wolfgang Tittel, “Efficient and long-lived zeeman-sublevel atomic population storage in an erbium-doped glass fiber”, *Physical Review B*, vol. 92, no. 24, pp. 241111, 2015.
- [29] Sara Shafiei, Erhan Saglamyurek, and Daniel Oblak, “Hour-long decay-time of erbium spins in an optical fiber at milli-kelvin temperatures”, in *Quantum Information and Measurement*. Optical Society of America, 2021, pp. F2A–4.
- [30] Eyal Buks, “Tunable multimode lasing in a fiber ring”, *Physical Review Applied*, vol. 19, no. 5, pp. L051001, 2023.
- [31] Nobuyuki Kagi, Akira Oyobe, and Kazunori Nakamura, “Temperature dependence of the gain in erbium-doped fibers”, *Journal of lightwave technology*, vol. 9, no. 2, pp. 261–265, 1991.
- [32] Pierluigi Franco, Michele Midrio, A Tozzato, Marco Romagnoli, and F Fontana, “Characterization and optimization criteria for filterless erbium-doped fiber lasers”, *JOSA B*, vol. 11, no. 6, pp. 1090–1097, 1994.
- [33] Emmanuel Desurvire and Jay R Simpson, “Evaluation of 4 i 15/2 and 4 i 13/2 stark-level energies in erbium-doped aluminosilicate glass fibers”, *Optics letters*, vol. 15, no. 10, pp. 547–549, 1990.
- [34] E Desurvire, JL Zyskind, and JR Simpson, “Spectral gain holeburning at 1.53 m in erbium-doped fiber amplifiers”, *IEEE Photon. Technol. Lett*, vol. 2, no. 4, pp. 246–248, 1990.
- [35] JL Zyskind, E Desurvire, JW Sulhoff, and DJ Di Giovanni, “Determination of homogeneous linewidth by spectral gain hole-burning in an erbium-doped fiber amplifier with geo/sub 2: Sio/sub 2/core”, *IEEE Photonics technology letters*, vol. 2, no. 12, pp. 869–871, 1990.
- [36] Robert K Hickernell, Kazumasa Takada, Makoto Yamada, Makoto Shimizu, and Masaharu Horiguchi, “Pump-induced dispersion of erbium-doped fiber measured by fourier-transform spectroscopy”, *Optics letters*, vol. 18, no. 1, pp. 19–21, 1993.
- [37] Herman A Haus, “Mode-locking of lasers”, *IEEE Journal of Selected Topics in Quantum Electronics*, vol. 6, no. 6, pp. 1173–1185, 2000.
- [38] A Liem, J Limpert, T Schreiber, M Reich, H Zellmer, A Tunnermann, A Carter, and K Tankala, “High power linearly polarized fiber laser”, in *Conference on Lasers and Electro-Optics*. Optica Publishing Group, 2004, p. CMS4.
- [39] D Crichton Hutchings, M Sheik-Bahae, David J Hagan, and Eric W Van Stryland, “Kramers-krönig relations in nonlinear optics”, *Optical and Quantum Electronics*, vol. 24, pp. 1–30, 1992.
- [40] Tianqi Sai, Matthias Saba, Eric R Dufresne, Ullrich Steiner, and Bodo D Wilts, “Designing refractive index fluids using the kramers–kronig relations”, *Faraday Discussions*, vol. 223, pp. 136–144, 2020.
- [41] John W Arkwright, P Elango, Graham R Atkins, T Whitbread, and JF Dignonnet, “Experimental and theoretical analysis of the resonant nonlinearity in ytterbium-doped fiber”, *Journal of lightwave technology*, vol. 16, no. 5, pp. 798–806, 1998.
- [42] George M Gehring, Robert W Boyd, Alexander L Gaeta,

- Daniel J Gauthier, and Alan E Willner, “Fiber-based slow-light technologies”, *Journal of Lightwave Technology*, vol. 26, no. 23, pp. 3752–3762, 2008.
- [43] Banoj Kumar Nayak and Eyal Buks, “Polarization-selective magneto-optical modulation”, *Journal of Applied Physics*, vol. 132, no. 19, pp. 193905, 2022.
- [44] Bernard Yurke and Eyal Buks, “Performance of cavity-parametric amplifiers, employing kerr nonlinearities, in the presence of two-photon loss”, *J. Lightwave Tech.*, vol. 24, pp. 5054–5066, 2006.
- [45] Gary Shaulov, *Modeling of mode-locked fiber lasers*, Rensselaer Polytechnic Institute, 1998.
- [46] V Roy, M Piche, F Babin, and GW Schinn, “Nonlinear wave mixing in a multilongitudinal-mode erbium-doped fiber laser”, *Optics express*, vol. 13, no. 18, pp. 6791–6797, 2005.
- [47] Marc-André Lapointe and Michel Piché, “Linewidth of high-power fiber lasers”, in *Photonics North 2009*. SPIE, 2009, vol. 7386, pp. 232–239.
- [48] Sergey A Babin, Dmitriy V Churkin, Arsen E Ismagulov, Sergey I Kablukov, and Evgeny V Podivilov, “Four-wave-mixing-induced turbulent spectral broadening in a long raman fiber laser”, *JOSA B*, vol. 24, no. 8, pp. 1729–1738, 2007.
- [49] Yujun Feng, Xiaojun Wang, Weiwei Ke, Yinhong Sun, Kai Zhang, Yi Ma, Tenglong Li, Yanshan Wang, and Juan Wu, “Spectral broadening in narrow linewidth, continuous-wave high power fiber amplifiers”, *Optics Communications*, vol. 403, pp. 155–161, 2017.
- [50] GR Lin and YC Lin, “Directly exfoliated and imprinted graphite nano-particle saturable absorber for passive mode-locking erbium-doped fiber laser”, *Laser Physics Letters*, vol. 8, no. 12, pp. 880, 2011.
- [51] Yung-Hsiang Lin and Gong-Ru Lin, “Kelly sideband variation and self four-wave-mixing in femtosecond fiber soliton laser mode-locked by multiple exfoliated graphite nano-particles”, *Laser Physics Letters*, vol. 10, no. 4, pp. 045109, 2013.
- [52] Nori Shibata, RALFP Braun, and ROBERTG Waarts, “Phase-mismatch dependence of efficiency of wave generation through four-wave mixing in a single-mode optical fiber”, *IEEE Journal of Quantum Electronics*, vol. 23, no. 7, pp. 1205–1210, 1987.
- [53] Thomas Schneider, *Nonlinear optics in telecommunications*, Springer Science & Business Media, 2004.
- [54] Hossein Taheri, Pascal Del’Haye, Ali A Eftekhar, Kurt Wiesenfeld, and Ali Adibi, “Self-synchronization phenomena in the lugiato-lefever equation”, *Physical Review A*, vol. 96, no. 1, pp. 013828, 2017.
- [55] Cyril Godey, Irina V Balakireva, Aurélien Coillet, and Yanne K Chembo, “Stability analysis of the spatiotemporal lugiato-lefever model for kerr optical frequency combs in the anomalous and normal dispersion regimes”, *Physical Review A*, vol. 89, no. 6, pp. 063814, 2014.
- [56] Alex McMillan, Yu-Ping Huang, Bryn Bell, Alex Clark, Prem Kumar, and John Rarity, “Four-wave mixing in single-mode optical fibers”, in *Experimental Methods in the Physical Sciences*, vol. 45, pp. 411–465. Elsevier, 2013.